

PAPER • OPEN ACCESS

Ab initio calculation of traction separation laws for a grain boundary in molybdenum with segregated C impurities

To cite this article: A M Tahir *et al* 2013 *Modelling Simul. Mater. Sci. Eng.* **21** 075005

View the [article online](#) for updates and enhancements.

You may also like

- [Influence of point defects on grain boundary mobility in bcc tungsten](#)
Valery Borovikov, Xian-Zhu Tang, Danny Perez *et al.*
- [Grain boundaries in bcc-Fe: a density-functional theory and tight-binding study](#)
Jingliang Wang, Georg K H Madsen and Ralf Drautz
- [Ab initio studies of two Al grain boundaries subjected to mixed tension/shear mode loading: how shear may promote breakage](#)
F J H Ehlers, M Seydou, D Tingaud *et al.*

***Ab initio* calculation of traction separation laws for a grain boundary in molybdenum with segregated C impurities**

A M Tahir, R Janisch and A Hartmaier

Interdisciplinary Centre for Advanced Materials Simulation, Ruhr-University Bochum, 44780 Bochum, Germany

E-mail: arshad.tahir@rub.de

Received 13 June 2013, in final form 18 July 2013

Published 6 September 2013

Online at stacks.iop.org/MSMSE/21/075005

Abstract

We have determined the influence of carbon on mechanical properties such as grain boundary energy, work of separation (WoS) and fracture strength of the $\Sigma 5(3\ 1\ 0)[0\ 0\ 1]$ symmetrical tilt grain boundary (STGB) in molybdenum with *ab initio* methods. From our *ab initio* results, we derived traction–separation laws that can be used in continuum simulations of fracture employing cohesive zones. Our results show that with an increasing number of C atoms at the grain boundary, the energy of the grain boundary is lowered, indicating a strong driving force for segregation. Uni-axial tensile tests of the grain boundary reveal that there is only a small effect of segregated C atoms on the cohesive energy or WoS of the grain boundary, while the strength of the $\Sigma 5(3\ 1\ 0)[0\ 0\ 1]$ STGB increases by almost 30% for a complete monolayer of C. This increase in strength is accompanied by an increase in grain boundary stiffness and a decrease of the interface excess volume. The characteristic parameters are combined in the concentration-dependent traction–separation laws. A study of the scaling behaviour of the different investigated systems shows that the energy–displacement curves can be well described by the universal binding energy relationship even for different C concentrations. These findings open the way for significant simplification of the calculation of *ab initio* traction separation laws for grain boundaries with and without impurities.

(Some figures may appear in colour only in the online journal)



Content from this work may be used under the terms of the [Creative Commons Attribution 3.0 licence](http://creativecommons.org/licenses/by/3.0/). Any further distribution of this work must maintain attribution to the author(s) and the title of the work, journal citation and DOI.

1. Introduction

Simulations of fracture rely on cohesive models which describe the physical process that causes separation of the material and that finally leads to the formation of free surfaces. Such commonly used continuum scale traction–separation laws have to combine different effects such as bond-breakage, plastic deformation and void growth when dealing with ductile materials. However, starting with brittle fracture, we can describe the separation process by interplanar potentials that can be calculated *ab initio* [1]. In the long run, we aim at an atomistically informed fracture model where the information about bond strength and cohesive energy will be obtained from *ab initio* calculations, whereas the elastic and plastic effects in the grain interior will be considered on the continuum level using, for instance, a crystal plasticity method.

Many examples of *ab initio* calculations of the strength of materials can be found in the literature. For reviews, see, e.g., [2, 3]. They are based on so-called *ab initio* tensile tests, which allow the calculation of not only the theoretical strength, but also the elastic constants. Thus, together with calculations of the work of separation (WoS) they provide a full characterization of the elastic properties of a material. If carried out in a ‘drag-like’ fashion under either a tensile or shear load, they are also suitable to identify failure mechanisms on the atomic scale [4, 5]. Furthermore, the application of multi-axial loading conditions reveals, e.g., the dependence of tensile strength on a shear load [6, 7], providing the basis for the application of realistic, three-dimensional loading conditions. Last but not least, the influence of alloying elements or impurities on the intrinsic strength can also be taken into account when deriving concentration-dependent traction–separation laws from *ab initio* fracture energies [8, 9]. As we have shown in a previous study [10], such *ab initio* traction–separation laws are useful for a systematic investigation of the influence of material parameters on crack growth in different microstructures under different loading conditions.

However, although these kind of calculations are well established, open questions remain when the results of tensile tests shall be transferred to the process of fracture. One problem is that the strength depends on the distribution of the elastic energy in the supercell. Unfortunately, the strain distribution during a homogeneous, fully relaxed computational tensile test—in which the strain distributes equally among a number of N crystallographic planes in the supercell perpendicular to the tensile axis—does not reflect the strain distribution in front of a crack tip. Furthermore, the continuation of a homogeneous tensile test beyond the inflection point finally leads to N freestanding layers. The energy of this configuration is different from the energy of two free surfaces, which is needed to calculate the WoS or cleavage energy. In a traction–separation law, however, the strength (the slope in the inflection point) and the WoS have to be related. Alternatively, the tensile test can be carried out in terms of rigid grain shifts [5, 11, 12]. Here the total strain is localized in a pre-defined cleavage plane. For small strain, a relaxation of the ions while keeping the total extension of the cell fixed after the rigid grain shift leads again to a homogeneous distribution of the strain in the cell, while for large strains (beyond the inflection point), the system relaxes towards the surface configurations. This strain distribution is still different from the $1/\sqrt{r}$ dependence in front of a crack tip, but the localization of strain is more realistic. Furthermore, the end-point of the energy–displacement curve is a well defined surface energy. However, the slope in the inflection point depends on the number of layers in the cell (which should be large to arrive at meaningful surface energies).

Nguyen and Ortiz [1] make use of the fact that in a relaxed calculation the elastic energy that is stored in the material changes the strength, but not the WoS, to establish a scaling-scheme for the maximum strength of a material. The picture behind this is that the elastic

energy which is released to break the system into two free surfaces is stored in a finite volume until it localizes at the cleavage plane. An asymptotic quadratic approximation is made for the relaxed energy–displacement curve to enable a simple scaling with the number of layers. The resulting traction–separation law is a triangle with the tip σ_{\max} at displacement $\Delta = \Delta_{\max}$ at which the asymptotic energy curve reaches the value of the surface energy, and the area under the traction–separation curve is the relaxed WoS. This scheme has the drawback that as the ‘elastic storage volume’ becomes large ($N \rightarrow \infty$), the strength of the material becomes zero.

This is overcome in the approach of Lazar and Podloucky [11, 12], who carry out rigid grain shifts followed by atomic relaxations and introduce finite localization lengths for both unrelaxed (l_b) and relaxed (L_b) cleavage. The charm of the approach is that L_b can be related to the unrelaxed, and hence size-independent, fracture properties. The disadvantage is that the unrelaxed cleavage energy that occurs in the relation then also involves the energy of unrelaxed surfaces, which is an ambiguous quantity.

In our approach, we combine size-independent and well-defined quantities by deriving the strength from an unrelaxed rigid-grain shift tensile test and demanding that the area under the traction–separation curve equals the relaxed WoS. The underlying assumption is that in front of a propagating crack the strain distribution is not that of a relaxed tensile test, but closer to the results of a rigid body displacement. After the crack has passed, however, the newly created free surfaces relax to their equilibrium configuration. The details of our procedure are given in sections 2 and 4.5.

As mentioned previously, both simulations of fracture involving cohesive zones as well as *ab initio* tensile tests via rigid-grain shifts require a pre-definition of the crack path/plane. In the paper at hand, we focus on failure along a grain boundary in Mo, because the assumption that this body-centred cubic (bcc) metal mainly fails due to grain boundary embrittlement is supported by experimental evidence. Furthermore, the intrinsic grain boundary brittleness of refractory metals can be enhanced or reduced significantly by segregated impurities; see, e.g., [13–16]. This knowledge can be used to optimize the material properties if one understands the mechanisms and effects of different impurity atoms [13, 17]. Thus our goal is to derive traction separation laws from *ab initio* results that reflect the influence of C on grain boundary strength in Mo.

Our model system is the $\Sigma 5(3\ 1\ 0)[0\ 0\ 1]$ symmetrical tilt grain boundary (STGB) in molybdenum which has been studied experimentally [18–20] and theoretically [21–24] quite extensively in the past. In the present study, the effect of C atoms on the strength of the $\Sigma 5(3\ 1\ 0)[0\ 0\ 1]$ STGB in Mo is investigated because of the abundance of C as an impurity element in most real material systems and the expected positive influence of C on the grain boundary strength [15, 16, 25, 26].

This paper is organized as follows. In section 2 the computational procedure, including an explanation of grain boundary nomenclature and details of performing ‘*ab initio* uni-axial tests’, is described. In section 3 the universal binding energy relationship (UBER) and its implications are reviewed. In section 4, results, i.e., the details about the lattice constant and bulk modulus of Mo obtained during present work are compared with the experimental values (4.1). Thereafter the grain boundary structure after a full optimization of the microscopic degrees of freedom (4.2) is discussed. Subsequently, the results of the uni-axial tests are presented in section 4.3. The scaling behaviour and fitting of the data of all the systems investigated is demonstrated in section 4.4, and the relationship between energies, strength and the effect of C on them is discussed in section 4.5. Finally, the observations and findings are concluded and summarized in section 5.

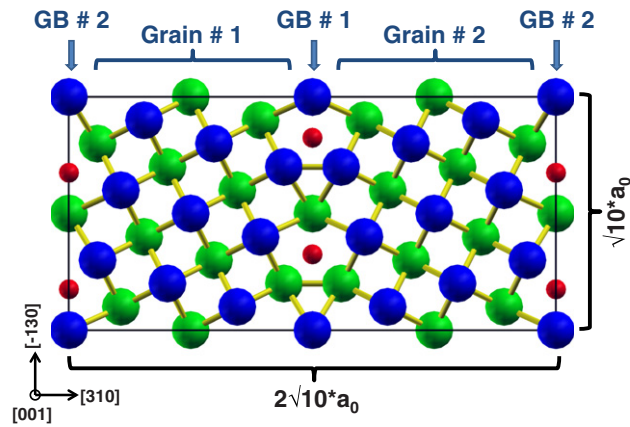


Figure 1. Structure of $\Sigma 5(310)[001]$ STGB. Blue and green atoms represent the Mo atoms from different layers in bcc structure and the small red atoms are C atoms present at the two grain boundaries in this super-cell structure. Due to periodicity, we see the GB#2 twice in this super-cell structure (colours online).

2. Technical details

The software used for *ab initio* density functional theory (DFT) calculations was the Vienna *Ab initio* Simulation Package (VASP) [27–29]. The exchange-correlation effects were approximated within the generalized gradient approximation (GGA) and ultra-soft pseudo-potentials [30] were used to describe the core–valence interaction. Convergence tests for the optimization of the k -point mesh and the energy cut-off for the plane wave basis set were performed. Thereafter, the equilibrium lattice constant for bcc Mo was calculated employing a $12 \times 12 \times 12$ k -point mesh of Monkhorst–Pack type. Subsequently, a $\Sigma 5(310)[001]$ STGB was constructed using a base centred orthorhombic super-cell with 20 atoms as shown in figure 1 (blue atoms). The unit vectors of the 20 atoms base centred orthorhombic cell are $(\frac{1}{2}\sqrt{10}, -\frac{1}{2}, 0)a_0$, $(\frac{1}{2}\sqrt{10}, \frac{1}{2}, 0)a_0$ and $(0, 0, 2\sqrt{10})a_0$, with a_0 being the lattice constant of bcc Mo. In this structure, the misorientation between the two grains, or, in other words, the tilt angle is 36.9° . In the nomenclature used above, Σ indicates that for the chosen misorientation a periodic superstructure can be found, the so-called coincidence site lattice (CSL). The value of Σ is the volume of a unit of this CSL divided by the volume of the bcc Mo unit cell, i.e., it is a measure for the periodicity of the grain boundary. The grain boundary plane is given in round brackets i.e. (310) , whereas the direction of the tilt axis is in rectangular ones, i.e., $[001]$.

In this supercell, the periodic images of the grain boundaries are separated by 10 layers of Mo atoms. The convergence of results wrt the cell size has been investigated by Ochs [31] who compared the site projected density of states of the grain boundary supercell and bulk supercell. The comparison showed that as one moves away from the grain boundary and reaches the fifth layer, the electronic density of states of the grain boundary supercell and the bulk supercell match, i.e., in the centre of the grain, bulk-like conditions are obtained. Furthermore, the grain boundary energy for two super-cells in Mo, i.e. 20 atoms supercell with GB to GB spacing of 10 layers (the same as the present work) and 40 atoms supercell with GB to GB spacing of 20 layers were calculated, and the difference observed was less than 10 mJ m^{-2} [31]. For our work, we also confirmed that during the tensile test the displacements in the grain interior after relaxation of the atomic positions equal that in a single-crystal unit cell in the same orientation (with the tensile axis along the $[310]$ -direction).

By construction, the tilt grain boundary considered here is symmetric, which means that the grain boundary plane divides the misorientation angle in two equal parts. In other words, it represents a mirror plane. This mirror symmetry is sometimes broken in the bcc transition metals, depending on the filling of the d -valence states [23, 24]. Thus, the stable translation state of the interface was obtained by rigid grain shifts followed by atomic relaxations in the three directions in our grain boundary, i.e., in the direction perpendicular to the interface [3 1 0], in the direction parallel to the interface [1 3 0] as well as in the direction of tilt axis, i.e., [0 0 1].

Uni-axial mechanical tests were performed on the $\Sigma 5(3\ 1\ 0)[0\ 0\ 1]$ STGB 20-atom super-cell employing a k -point mesh of $6 \times 6 \times 2$. For this purpose, initially the unit vector length along [3 1 0] was decreased (increased) stepwise and only the grain boundary separation (between Grain#1 and GB#1 and to have periodicity in the structure, separation between Grain#2 and GB#2) was contracted (expanded) to compensate for this change in length. In other words, the two grains were shifted rigidly relative to each other in certain steps. The maximum shift employed was until -10% ($+50\%$) of the super-cell length along [3 1 0]. Subsequently, the structures were allowed to relax while keeping the vector length fixed. In this way, we can model an ideally brittle fracture under loading mode I.

The next aim was to introduce C atoms at the grain boundary which is the preferred segregation site for impurity atoms and has been determined previously by Janisch *et al* [32]. For this purpose, an orthorhombic primitive 80-atom (blue and green atoms shown in figure 1) super-cell was constructed from the 20-atom (blue atoms only) super-cell by multiplying the latter by 4 along the [0 0 1] direction, i.e., the direction of the tilt axis. Thus, the grain boundary area in the super-cell increased by a factor of 4 and interstitial positions for up to 4 C atoms per grain boundary are provided. Calculations were performed with varying C contents. Initially, all the available four positions per grain boundary were filled with four C atoms forming a complete mono-layer and the atoms were allowed to relax at their positions as well in order to find out the stable position of the C atoms at the grain boundary. Subsequently, the number of C atoms per grain boundary were reduced to 3, 2 and finally 1 C atom. The k -point mesh used for the orthorhombic primitive 80-atom grain boundary super-cell was $8 \times 4 \times 2$. The pure Mo bulk structure using the same number of atoms in the super-cell was also constructed in order to find out the energy of the grain boundary i.e. γ using the relation:

$$\gamma = \frac{E_{\text{tot},GB}^{\text{Mo+mC}} - nE_{\text{Mo}}^{\text{bulk}} - mE_C}{2A}, \quad (1)$$

where $E_{\text{tot},GB}^{\text{Mo+mC}}$ is the total energy of the grain boundary super-cell containing a certain number of C atoms, $nE_{\text{Mo}}^{\text{bulk}}$ is the energy of the same number of Mo atoms in bulk condition and mE_C is the reference energy of the same number of C atoms as at the grain boundary. E_C varies from -9.27 eV for graphite to -7.67 eV as an interstitial atom in a $2 \times 2 \times 2$ bcc Mo supercell. The reference energy of C in diamond (i.e. -9.12 eV) which has been used in the present work lies within the values of C as graphite and C as an interstitial atom. The energy of the (3 1 0) surface was also calculated in both cases i.e. for the 20-atom base centred orthorhombic super-cell as well as the 80-atom orthorhombic primitive super-cell. The energy–displacement data obtained after DFT calculations was evaluated and the work required to separate the two surfaces i.e. the work of separation (WoS) was determined according to

$$\text{WoS} = \frac{2 \cdot E_{\text{tot}}^{\text{FS}} - E_{\text{tot},GB}^{\text{Mo+mC}}}{2A}, \quad (2)$$

where $E_{\text{tot}}^{\text{FS}}$ is the energy of free surface slab with equilibrium partitioning of C atoms on the two surfaces (described in section 4.3) in the respective grain boundary. As described in detail in section 3, the energy–displacement data was also fitted using the UBER [33]. The derivative of

the obtained data gives us the traction separation data which can be used for the cohesive zone model at continuum level using the finite element method. From the energy–displacement data, the theoretical strength σ_{th} of the interface can be calculated as the slope at the inflection point,

$$\sigma_{th} = \left. \frac{dE}{d\Delta} \right|_{E''(\Delta)=0}, \quad (3)$$

where Δ is the displacement from the equilibrium inter-planar distance [5].

3. Scaling behaviour

According to Rose *et al* [33], the cohesive energies or binding energies E_b of metals have a universal form. This phenomenon has been observed for adhesion [34] and cohesion [35] of metals, as well as chemisorption on metal surfaces [36]. Hayes *et al* [37] have even observed similar universal behaviour of energy–displacement curves for the non-metallic systems (Al_2O_3 and Si). More recently, Janisch *et al* [5] have observed the universal behaviour for geometrically different grain boundaries in aluminum. In section 4.4, we are able to show that it also holds for grain boundaries in Mo having different C contents. This apparent universality of the equation of state of chemically or geometrically different systems means that we can determine the cohesive behaviour of any material from three parameters, E_b^e , d_0 , and $E_b''(d_0)$, (i.e. the equilibrium binding energy, the equilibrium separation and elastic modulus at equilibrium separation respectively) once the functional form $g(a)$ is known in the relation,

$$E_b(d) = |E_b^e|g(a). \quad (4)$$

The absolute value of the equilibrium binding energy, i.e., $|E_b^e|$ is called WoS in the present publication. Here d is the inter-atomic separation, or, in the case of interface energies, the inter-planar distance and a is the rescaled separation,

$$a = \frac{\Delta}{l}. \quad (5)$$

The characteristic length scale l depends on the curvature of the energy–displacement curve at the minimum, i.e., on the inter-planar elastic modulus:

$$l = \sqrt{\frac{|E_b^e|}{E_b''(d_0)}}. \quad (6)$$

The function used for the fitting of the uni-axial test results has the form

$$g(a) = -(1+a)e^{-a}. \quad (7)$$

The same function was also used by Rose to represent the results of displacing metal–metal interfaces of different metals. In the present work, this function worked well only for rigid grain shift results. After the relaxation of the ionic positions, a few deviations were observed, which was attempted to overcome by using a polynomial function including higher order terms as explained in section 4.4.

4. Results

4.1. Lattice constant and bulk modulus of molybdenum

Using the available experimental value for the lattice constant of Mo, i.e., 3.15 (Å) as a starting point, the energy of a primitive unit cell of Mo was calculated for 10 different lattice constants

Table 1. Comparison between experimental (room temperature) and theoretical results of lattice constant and bulk modulus of Mo.

Parameters	This work	Experimental data
a_0 (Å)	3.153	3.147 [39], 3.150 [40]
Bulk modulus (GPa)	257.6	259 [41], 269 [42]

in order to determine the equilibrium DFT-lattice constant. The obtained results were fitted using the Murnaghan equation of state [38],

$$E_b(V) = C_b + \frac{B_0 V}{B'_0} \left[\frac{(V_0/V)^{B'_0}}{B'_0 - 1} + 1 \right] - \frac{V_0 B_0}{B'_0 - 1}, \quad (8)$$

in which C_b is a constant, V is the volume and V_0 is the equilibrium volume, B_0 and B'_0 are the bulk modulus and its derivative at equilibrium volume, respectively. Table 1 shows the comparison between experimental (room temperature) and calculated values of lattice constant and bulk modulus of Mo. The lattice constant obtained during the present work shows a very good agreement with the experimental values. The value for the bulk modulus is also in good agreement with the experimental values considering the fact that roughly 10% deviation in the value of bulk modulus is quite normal in the available literature [41, 42] and that the *ab initio* calculated results are applicable to 0 K.

4.2. Grain boundary structure and energy

Initially the grain boundary structure of the $\Sigma 5(3\ 1\ 0)[0\ 0\ 1]$ STGB was constructed considering the macroscopic parameters, i.e., using the perfect lattice dimensions. As shown in figure 1, GB#1 is in between the two grains whereas the GB#2 is the second grain boundary which can be seen twice due to the periodic boundary conditions. In such a construction, the atoms of the grain boundary plane and of the planes next to the grain boundary come unnaturally close to or far away from each other. Therefore, the microscopic degrees of freedom of the grain boundary were optimized and rigid grain shifts were performed perpendicular as well as parallel to the interface followed by the relaxation of the atomic positions using the base centred orthorhombic super-cell containing 20 atoms. The grain boundary exhibits an excess volume of roughly 2.4% perpendicular to the interface, i.e., in the $[3\ 1\ 0]$ direction. Also the mirror symmetry along the tilt axis, i.e., the $[0\ 0\ 1]$ direction, was broken and a shift of roughly 9% of each grain was observed for the pure Mo grain boundary. This is in agreement with the results of previous calculations [23, 24]. In the citations mentioned, Ochs *et al* have argued that this effect is due to the half filling of the Mo d-states which results in a spherical electron distribution around the atoms. With such an electronic distribution, the grain boundary structure with broken mirror symmetry, which is more compact, is lower in energy than the mirror symmetric grain boundary structure which is favoured by directional bonds [13]. However, as soon as a C atom was placed at the grain boundary, the shift along $[0\ 0\ 1]$ vanished upon relaxation of the atomic positions, and the mirror symmetry was restored. The reason behind this is that C preferentially forms angle-dependent bonds with covalent character and hence favours the mirror-symmetric configuration of the STGB in Mo [13], in which it can be placed in an open structural unit. The shifts obtained were then used for an orthorhombic primitive 80-atom super-cell in which we had the flexibility of placing a maximum of 4 C atoms per grain boundary. The resulting grain boundary structure is in agreement with that of experimental observations and previous calculations [23, 32]. In this work, the number of carbon atoms (1–4) at the interface corresponds to a coverage of one-fourth to a complete monolayer. The concentration limit until which the segregation process is favourable is two mono-layers of C atoms, as observed

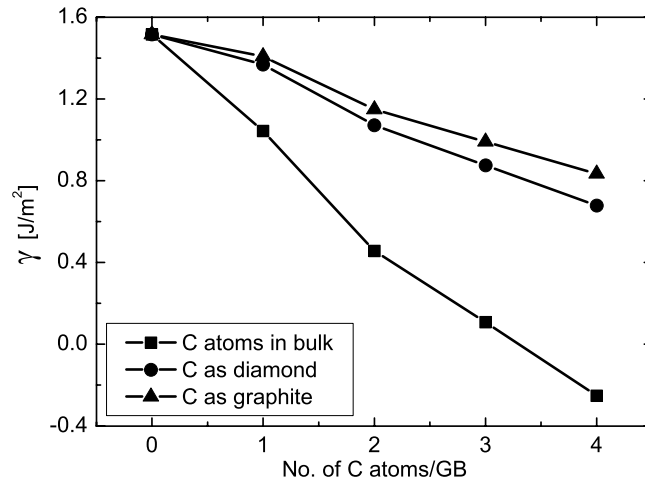


Figure 2. Energy of grain boundary versus C content for three different chemical potentials of C.

by Janisch *et al* [43]. That study shows that as long as interface energy decreases with an increasing number of C atoms at the grain boundary, the segregation energy remains negative, which is a sign of the grain boundary being an attractive site for segregation of C atoms.

The energy of the grain boundary has been calculated as a function of C content using equation (1) with three different chemical potentials of C, namely C in the graphite or diamond phase, and interstitial C atoms in a bulk supercell of the same size as the grain boundary cell. The results are shown in figure 2. In all cases, the energy of the grain boundary decreases with increasing numbers of C atoms per grain boundary, but with a different slope for the different chemical potentials. The grain boundary energy based upon interstitial C atoms in Mo bulk initially is the most well-defined one, because it includes neither the solution enthalpy of C in Mo nor the segregation energy in the energy of formation of the grain boundary (as is the case with the other two chemical potentials). However, it decreases down to a negative value at a concentration representing a coverage of the interface with one complete monolayer of C. In this case, the local concentration of C is far above the solubility in the bulk, leading to an unphysically high chemical potential and correspondingly low grain boundary energy. With graphite, the most stable phase of C, the change in the grain boundary energy is lowest. This variation of grain boundary energy with chemical potential shows that the coverage of the grain boundary can be enhanced by a factor of four even at a constant grain boundary energy (e.g., around 1 J m^{-1}) by varying the chemical potential, which in an experiment can be done by changing the C partial pressure. The grain boundary energy with the chemical potential of C in the diamond phase is tabulated in the table 2. In this case, the energy of the grain boundary is lowered by more than 50% with increasing numbers of C atoms which tells us that the grain boundary is attractive for segregating C. This does not necessarily mean that cohesion between two grains (or WoS) also increases with increasing numbers of C atoms, because the presence of C not only affects $E_{\text{tot,GB}}^{\text{Mo+mC}}$, but also $E_{\text{tot}}^{\text{FS}}$ in equation (2). In fact, we observed almost no effect on the WoS as explained in the next section.

4.3. Energy-displacement curves

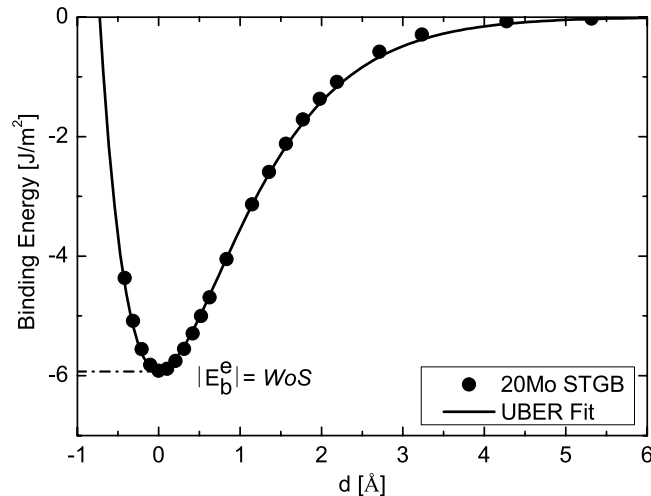
Before performing the uni-axial tests on the optimized grain boundary structures, the most favorable distribution of the C atoms on the two (3 1 0) surfaces after cleavage was determined.

Table 2. Interface energy γ , work of separation WoS , grain boundary expansion ΔL and the elastic modulus $E_b''(d_0)$ of Mo bulk and STGB in Mo having a certain number of C atoms at the grain boundary (relaxed results).

	γ ($J m^{-2}$)	WoS ($J m^{-2}$)	ΔL (\AA)	$E_b''(d_0)$ ($GPa \text{\AA}^{-1}$)
Pure bulk Mo (310) plane	—	6.23	—	43.9
Pure Mo STGB	1.52	4.71	0.46	31.1
Mo STGB with 1 C atom	1.37	4.70	0.30	37.2
Mo STGB with 2 C atoms	1.07	4.77	0.28	37.2
Mo STGB with 3 C atoms	0.87	4.78	0.08	38.8
Mo STGB with 4 C atoms	0.68	4.77	0.05	41.1

Table 3. Energy of free (3 1 0) surfaces having different distributions, n-mC, of C atoms, where n and m are the number of C atoms on surfaces one and two, respectively.

Configurations	Energy (eV)	Energy Difference (eV)
4-0C	-448.46	0.00
3-1C	-447.38	1.08
2-2C	-446.66	1.80

**Figure 3.** Binding energy versus separation of 20Mo STGB supercell.

The results in table 3 show that all 4 C atoms always prefer to stay on one of the two new surfaces formed. Similar behaviour was observed for lower concentrations of C atoms. With the fully relaxed supercell, uni-axial tests were performed as explained in section 2 for pure Mo as well as Mo containing C atoms at the grain boundary. Initially a rigid grain shift was given at a defined cleavage plane next to the grain boundary. In the second step, atoms were allowed to relax and corresponding energies were obtained. As an example, the results for a 20 atom molybdenum supercell in which the two grains were shifted relative to each other along the [3 1 0] direction is shown in figure 3. The minimum of the curve gives us the equilibrium binding energy and the zero level of energy represents twice the surface energy.

Results for the investigated systems show that the presence of C changes the minimum of the curve, i.e., WoS of the grain boundary between 5.91 and $6.12 J m^{-2}$ for the pure grain

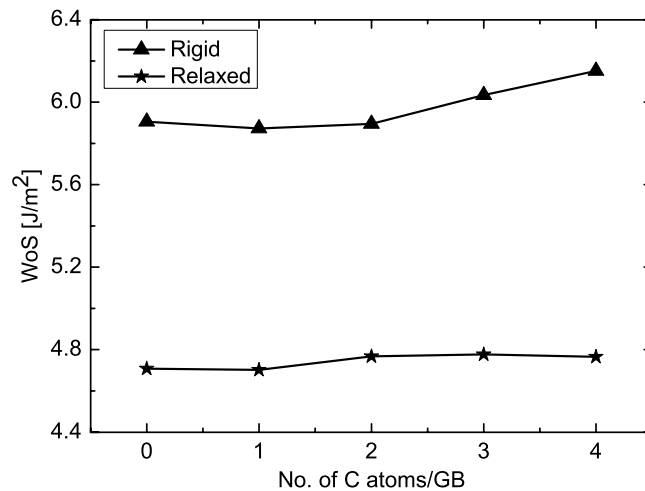


Figure 4. Effect of C on the work of separation.

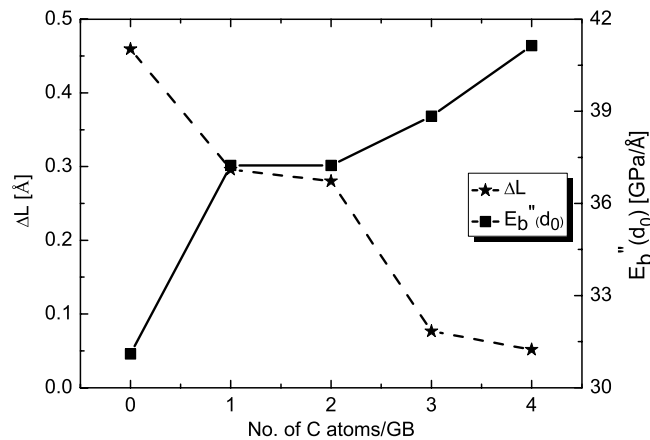


Figure 5. Grain boundary expansion ΔL and elastic modulus $E_b''(d_0)$ as a function of number of C atoms per grain boundary.

boundary to complete monolayer formation of C in the rigid case and from 4.71 to 4.77 J m⁻² in the relaxed case. The WoS as a function of the number of C atoms at the grain boundary is shown in figure 4. In the rigid case, a slight increase is observable at higher C contents, however, after atomic relaxation of the surface structures, a more or less constant value of WoS is observed.

The introduction of C not only affects E_b^c , but also d_0 , which means a change in excess volume of the grain boundary along the [3 1 0] direction. The expansion (ΔL) of the pure and C segregated grain boundary has been obtained relative to bulk Mo with the same number of interstitial C atoms on octahedral sites as at the grain boundary, and is shown in figure 5 and table 2. The introduction of C at the grain boundary structure slightly increases the total volume of the supercell, but less than in the bulk supercell of the same kind. Thus, the overall trend shows a decreasing excess volume with an increasing number of C atoms at the interface. This is accompanied by an increase in the elastic modulus of the interface, the second derivative of the energy–displacement function at the minimum. The presence of C at the grain boundary

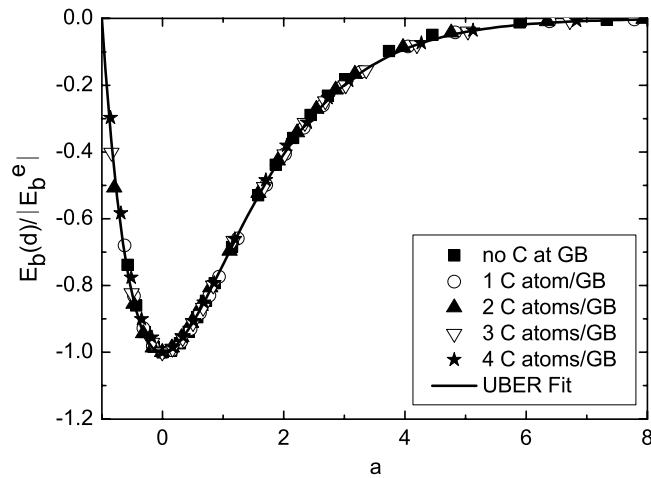


Figure 6. Rigid grain shift energy displacement relationships re-scaled according to equations (4)–(6), using equation (7).

makes the interface more stiff, however, the elastic modulus for (3 1 0) Mo bulk plane is still higher than that of all the grain boundary structures.

4.4. Scaling and fitting of the data

As mentioned in section 3, a universal behaviour of materials under strain has been shown for bulk metals and ceramics and for coherent metal–metal interfaces. In the present work, we probe this universality for our Mo grain boundary with different C contents. As shown in figure 6, the results after rigid grain shifts scale perfectly onto one curve. Moreover, the data points are very well described by the function given in equation (7).

In contrast, in the case of rigid grain shifts followed by atomic relaxations, the function given in equation (7) does not describe the results well. Therefore, for all different systems investigated, the relaxed data near the minimum (from -5% compression until 5% tension) was fitted using a cubic function and the values for E_b^c and d_0 were obtained. The value of $E_b''(d_0)$ was obtained from the second derivative of the respective cubic functions. The relaxed results were then rescaled as shown in figure 7 using the obtained cubic fit results. For the fitting of the whole relaxed energy displacement curve, different higher order polynomials were tried, but it was observed that the best fit could be obtained by using equation (9). The fit could not be further improved by using only the physical parameters i.e. $E_b''(d_0)$ and d_0 .

$$g(a) = -(1 + a - 0.079a^3 + 0.0063a^4 + 0.0002a^5)e^{-a}. \quad (9)$$

However, apart from a few outliers the agreement is satisfactory. On the one hand, the deviations occur close to the critical displacement where the structure becomes unstable and where we can think of de-bonding or crack formation. On the other hand, there is some deviation in the highly compressed regions, but the fact that the bcc transition metals do not obey a universal scaling law under compression has already been pointed out by Qin *et al* [44].

4.5. Fracture strength and traction–separation laws

The derivative of the energy–displacement data yields the traction separation curve (continuous line) as shown in figure 8 for the 20 Mo bulk (3 1 0) plane rigid case. To use this data in a

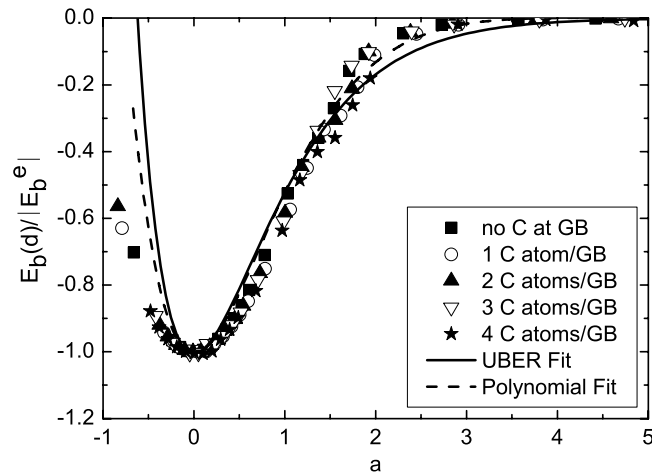


Figure 7. Energy displacement relationships with relaxed atomic positions, re-scaled according to equations (4)–(6), using equation (9).

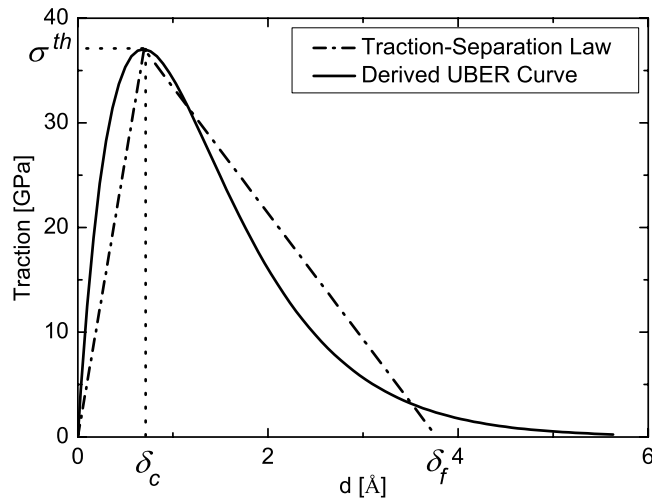


Figure 8. Derivative of UBER curve fitted to DFT results and traction–separation triangle for the 20 Mo (3 1 0) bulk plane (rigid).

cohesive zone model for the grain boundary, we define a triangle which is given by the origin, the maximum strength (σ_{th}) at the critical separation δ_c , and the requirement that the area under the curve equals the WoS. From the latter we can derive the the final separation δ_f , the displacement at which the two cohesive surfaces are completely separated, via

$$\delta_f = \frac{2WoS}{\sigma_{th}}. \quad (10)$$

The traction separation laws for different C contents are shown in figure 9, and the defining parameters δ_c and δ_f as a function of C concentration are plotted in figure 10. The decrease in the values of δ_c and δ_f is again evidence of increased stiffness due to the presence of C.

The quantitative results for rigid grain shift calculations have been summarized in table 4 for the different systems investigated. As can be seen, as soon as C enters the grain boundary,

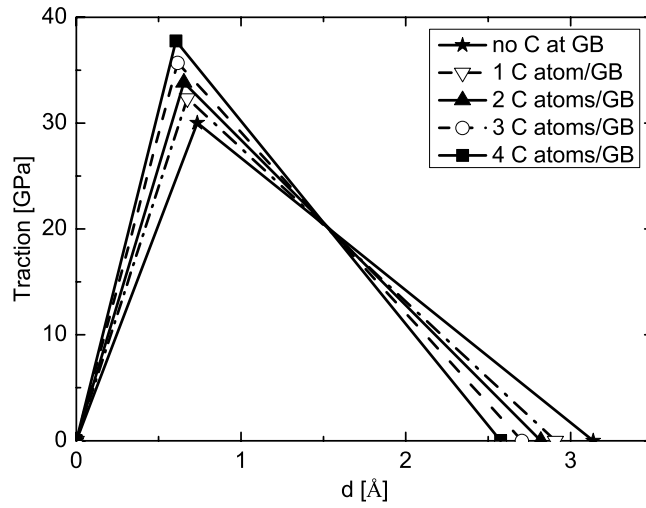


Figure 9. Traction-separation triangles as a function of number of C atoms per GB.

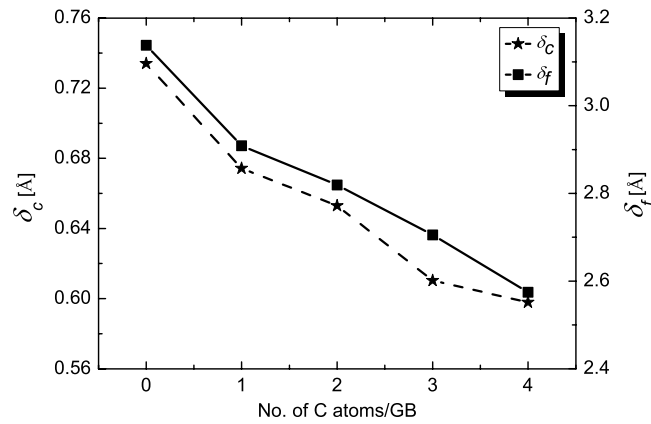


Figure 10. Critical separation δ_c and final separation δ_f as a function of number of C atoms per GB.

Table 4. Fracture strength σ_{th} , Critical separation δ_c and the final separation δ_f of Mo bulk and STGB in Mo having a certain number of C atoms at the grain boundary (rigid results).

	σ_{th} (GPa)	δ_c (Å)	δ_f (Å)
Pure bulk Mo (3 1 0) plane	37	0.70	3.78
Pure Mo STGB	30	0.73	3.14
Mo STGB with 1 C atom	32	0.67	2.91
Mo STGB with 2 C atoms	34	0.65	2.82
Mo STGB with 3 C atoms	35	0.61	2.71
Mo STGB with 4 C atoms	37	0.60	2.57

the strength starts to increase up to the formation of a complete monolayer. At this coverage the obtained fracture strength of the grain boundary equals the strength of pure bulk Mo if loaded perpendicular to the (3 1 0) plane (table 4).

As mentioned before, C preferentially forms angle dependent bonds with covalent character with the nearest neighbour host metal atoms. When placed at the interface, it increases

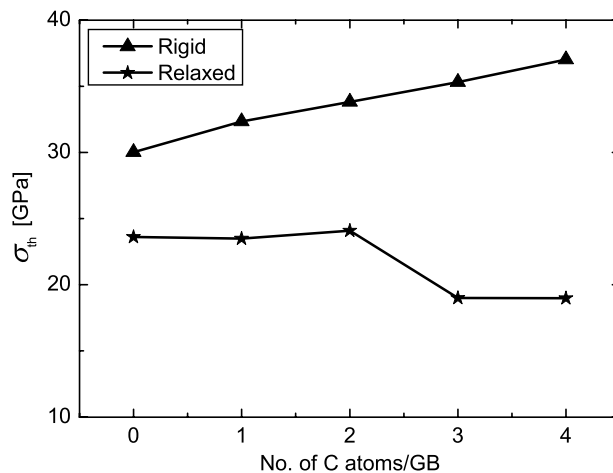


Figure 11. Effect of C on the fracture strength of the grain boundary.

the stiffness of the grain boundary layer and decreases the excess volume of the system. Thus rigid strength increases continuously with increasing C content; see figure 11. The relaxed strength, however, saturates and decreases, since upon relaxation the strain distributes in the supercell and it is the overall stiffness of the cell, not only the grain boundary layer, which determines the strength. This overall stiffness is reduced, because some charge of the Mo–Mo bonds is redistributed into the Mo–C bonds. To get an impression of this chemical effect of C on the strength of the neighbouring layers, we also carried out a tensile test in which the cleavage plane was one crystallographic layer away from the grain boundary. For one monolayer of C at the grain boundary, the next interplanar strength was reduced to a value slightly below the bulk value of 37 GPa. However, this is still well above the strength of the pure grain boundary, so the overall strength of the bicrystal is enhanced. We note, however, that the elastic energy that is stored in the grains during a real fracture process does not enter our traction–separation laws, since our goal is to describe effects due to this energy in the continuum model outside the cohesive zone. The saturation behaviour of the relaxed strength in figure 11 indicates already that as the excess volume approaches zero (figure 5) the far-field elastic distortions in the grain could also reduce the overall strength. Thus, the beneficial effect of C should not be extrapolated to higher concentrations without further investigations. If the focus is not on the simulation of fracture, but on mimicking a homogeneous tensile test, the influence of relaxations on the (homogeneous) tensile strength of a grain boundary with segregated C impurities can be extracted by referring the energy–displacement values to those of a corresponding bulk supercell. Although we already performed the first steps of such an investigation for the calculation of the excess volume, this shall be the topic of a different paper. Furthermore, tensile tests carried out in a ‘drag-like’ fashion [5], comparable to the shear calculations of Hamilton *et al* [4], will serve to identify details of the deformation mechanisms at special grain boundaries, apart from the mere bond-breaking process. Such details will be valuable information for a continuum material model outside the cohesive zone.

5. Summary and conclusions

Ab initio density functional theory calculations have been performed to obtain the cohesive zone parameters for a mesoscopic model describing intergranular fracture including the

effect of C impurities. Four different C concentrations (one-fourth to one monolayer of C at the interface) have been investigated during the present study and it has been observed that, independent of its chemical potential, C considerably lowers the grain boundary energy, indicating a strong driving force for segregation of C [43]. We find that the work of separation remains widely unaffected by the presence of C at the grain boundary, because the energy of the surfaces created by the separation is also lowered by the presence of C. In contrast, the fracture strength of the grain boundary, as revealed by a rigid-grain shift *ab initio* tensile test, shows a clear strengthening effect of C. This is accompanied by a reduction of the excess volume and an increase in stiffness of the interface.

These different trends in the work of separation and strength are consolidated in concentration-dependent traction–separation laws which are based on both quantities and the critical separation for fracture. We conclude that constitutive relationships including work of separation and strength are superior to commonly used energy-based fracture models (e.g. the Griffith criterion), even for brittle fracture. In any case, our results clearly indicate that the work of separation (from *ab initio* calculations) alone is not sufficient to describe fracture processes.

The energy–displacement curves for the different systems investigated here exhibit a scaling behaviour with only three parameters. Thus it is not necessary to perform calculations for the complete range of displacements of the grain boundary in future investigations. Once the analytical function for the binding-energy relationship has been determined, we can derive the strength from the equilibrium work of separation, the position of the energy minimum (related to the excess volume) and the curvature at the minimum (the interface stiffness).

Acknowledgments

AT acknowledges financial support through the German Research Foundation (DFG grant number JA-1079/4). This work has been carried out at ICAMS. ICAMS is supported through Thyssen Krupp AG, Bayer Material Science AG, Salzgitter Mannesmann Forschung GmbH, Robert Bosch GmbH, Benteler Stahl/Rohr GmbH, Bayer Technology Services GmbH and the state of North-Rhine Westphalia as well as the European Commission in the framework of the European Regional Development Fund (ERDF).

References

- [1] Nguyen O and Ortiz M 2002 *J. Mech. Phys. Solids* **50** 1727
- [2] Ogata S, Umeno Y and Kohyama M 2009 *Modelling Simul. Mater. Sci.* **17** 013001
- [3] Šob M, Friák M, Legut D, Fiala J and Vitek V 2004 *Mater. Sci. Eng. A* **387–389** 148
- [4] Hamilton J C and Foiles S M 2002 *Phys. Rev. B* **65** 064104
- [5] Janisch R, Ahmed N and Hartmaier A 2010 *Phys. Rev. B* **81** 184108
- [6] Černý M and Pokluda J 2007 *Phys. Rev. B* **76** 024115
- [7] Černý M and Pokluda J 2009 *J. Phys.: Condens. Matter* **21** 145406
- [8] Jiang D E and Carter E A 2004 *Acta Mater.* **52** 4801
- [9] Serebrinsky S, Carter E A and Ortiz M 2004 *J. Mech. Phys. Solids* **52** 2403
- [10] Prechtel M, Ronda P L, Janisch R, Hartmaier A, Leugering G, Steinmann P and Stingl M 2011 *Int. J. Fract.* **168** 15
- [11] Lazar P, Podloucky R and Wolf W 2005 *Appl. Phys. Lett.* **87** 261910
- [12] Lazar P and Podloucky R 2008 *Phys. Rev. B* **78** 104114
- [13] Janisch R and Elsässes C 2003 *Phys. Rev. B* **67** 224101
- [14] Geng W T, Freeman A J, Wu R and Olson G B 2000 *Phys. Rev. B* **62** 6208
- [15] Jardin J M, Kobylanski A and Goux C 1975 *C. R. Acad. Sci. Paris C* **280** 717
- [16] Kumar A and Eyre B L 1980 *Proc. R. Soc. Lond. A* **370** 431

- [17] Janisch R and Elsässer C 2009 *Int. J. Mater. Res.* **100** 1488
- [18] Pénişson J M, Bacia M and Biscondi M 1996 *Phil. Mag. A* **73** 859
- [19] Morita K and Nakashima H 1997 *Mater. Sci. Eng. A* **1053** 234
- [20] Campbell G H, Belak J and Moriarty J A 1999 *Acta. Metall. Mater.* **47** 3977
- [21] Marionopoulos A G, Vitek V and Carlsson A E 1995 *Phil. Mag. A* **72** 1311
- [22] Bacia M, Morillo J, Pénişson J M and Pontikis V 1997 *Phil. Mag. A* **76** 945
- [23] Ochs T, Beck O, Elsässer C and Meyer B 2000 *Phil. Mag. A* **80** 351
- [24] Ochs T, Elsässer C, Mrovec M, Vitek V, Belak J and Moriarty J 2000 *Phil. Mag. A* **80** 2405
- [25] Kurishita H, Oishi A, Kubo H and Yoshinaga H 1985 *Trans. Japan Inst. Met.* **26** 341
- [26] Hiraoka Y 1990 *Trans. Japan Inst. Met.* **31** 861
- [27] Kresse G and Hafner J 1993 *Phys. Rev. B* **48** 13115
- [28] Kresse G and Furthmüller J 1996 *Comput. Mater. Sci.* **6** 15
- [29] Kresse G and Furthmüller J 1996 *Phys. Rev. B* **54** 11169
- [30] Vanderbilt D 1990 *Phys. Rev. B* **41** 7892
- [31] Ochs T 2001 *Theoretische Untersuchungen der atomaren und elektronischen Struktur an Korngrenzen in kubisch raumzentrierten Übergangsmetallen und an Metall/Keramik-Grenzflächen* (Göttingen: Cuveillier)
- [32] Janisch R, Ochs T, Merkle A and Elsässer C 2000 *Mater. Res. Soc. Symp. Proc.* **578** 405–10
- [33] Rose J H, Smith J R and Ferrante J 1983 *Phys. Rev. B* **28** 1835
- [34] Ferrante J and Smith J R 1979 *Phys. Rev. B* **19** 3911
- [35] Rose J H, Smith J R, Guinea F and Ferrante J 1984 *Phys. Rev. B* **29** 2963
- [36] Smith J R, Ferrante J and Rose J H 1982 *Phys. Rev. B* **25** 1419
- [37] Hayes R L, Ortiz M and Carter E A 2004 *Phys. Rev. B* **69** 172104
- [38] Tyuterev V G and Vast N 2006 *Comput. Mater. Sci.* **38** 350
- [39] Kittel C 1996 *Introduction to Solid State Physics* (New York: Wiley)
- [40] Donohue J 1974 *The Structure of the Elements* (New York: Wiley) pp 191–9
- [41] Dickinson J M and Armstrong P E 1967 *J. Appl. Phys.* **38** 602–11
- [42] Bolef D I and Klerk J D 1962 *J. Appl. Phys.* **33** 2311–4
- [43] Janisch R and Elsässer C 2008 *Phys. Rev. B* **77** 094118
- [44] Qin T, Drautz R and Pettifor D G 2008 *Phys. Rev. B* **78** 2141081